JOURNAL OF PROPULSION AND POWER
Vol. 26, No. 6, November–December 2010

Laser Pulsejet with Beam Concentration by Multiple Reflections in a Sharp-Cone Nozzle

Koichi Mori*
Nagoya University, Nagoya 464-8603, Japan
and
Hiroshi Katsurayama†
Yamaguchi University, Ube 755-8611, Japan

DOI: 10.2514/1.46939

A sharp cone is employed as a nozzle for pulsed laser propulsion. A laser beam is concentrated by multiple reflections inside of the cone to generate plasma. Impulse measurements reveal that a large momentum-coupling coefficient, around 0.3 mNs/J, is achieved. By comparing the experimental and computational impulses, 15% of the laser pulse energy is found to be converted to the internal and kinetic energies of gas inside of the blast wave. This estimation of energy efficiency is supported by ray-tracing analysis of the cone and other experimental results of the energy efficiency. Moreover, the conical nozzle is found to be tolerant to optical misalignment.

Nomenclature

C_m = momentum-coupling coefficient defined as ratio of impulse to laser pulse energy
E_{bw} = blast-wave energy defined as total amount of internal and kinetic energy of gas inside a blast wave
E_i = laser pulse energy
F = laser fluence
F_A = laser fluence at a point A on nozzle surface
F_i = laser fluence of incident laser beam
L_n = chord length of nozzle
p_a = ambient air pressure
r_k = ratio defined as $X_{Pk}/X_{P(k-1)}$
$\tilde{r}_n$ = dimensionless nozzle length defined as $L_n/\sqrt[3]{2\eta_{\mathrm{bw}}E_i/p_a(1-\cos\alpha_c)}$
X_P = axial position of point P on nozzle surface
α_c = half-cone angle of conical nozzle
α_j = angle of ray at jth reflection point
γ = specific heat ratio
η_{bw} = blast-wave energy efficiency defined as E_{bw}/E_i
η_{ref} = fraction of laser pulse energy E_i reflected on surface
θ_i = incident angle of laser beam

I. Introduction

IN ATMOSPHERIC flight driven by pulsed laser propulsion, a repetitively pulsed laser beam is irradiated remotely to a nozzle on the vehicle. The wall surface inside of the nozzle has a mirror finish to work as a focusing optic. The beam is focused to create plasma on a surface made of ablative or nonablative materials. Plasma, after created, is heated and further ionized by absorbing the laser power. Quick expansion of the plasma generates a blast wave. Impulsive thrust is imparted to the nozzle surface where the blast wave is deflected. The design of the nozzle in the optimum shape is crucial to extend the speed and altitude records of the laser-propelled vehicles. The nozzle must work as both a blast-wave deflector and as a beam concentrator. Thrust performance has been investigated for the different geometries of a nozzle: spike [1], cylinder [2,3], parabolic shell of revolution [4–7], and cone [7–9]. The momentum-coupling coefficient C_m stands for the thrust performance by a single laser pulse. Among the nozzle geometries investigated, the maximum record of C_m, as large as 0.5 Ns/mJ, has been attained by conical nozzles without using such ablative materials as Delrin. Its scaling law has been investigated in previous studies [7–9]; C_m is determined by the dimensionless nozzle length $\tilde{r}_n$ and the half-cone angle α_c. C_m increases with decreasing α_c for a given value of $\tilde{r}_n$. In all of the previous experiments for conical nozzles, an external focusing optic is used to concentrate a laser beam to generate plasma. In the experiments for the other shapes of the nozzle [1–7], the laser beam is reflected on the nozzle surface and is concentrated. In the nozzles of the parabolic shell of revolution [4–7], the laser beam is reflected on the inner surface of the shell and focused at the geometrical focal point where an ignition pin is placed. In the spike nozzles [1], the laser beam is reflected on the surface of the parabolic-shaped spike nozzle, and it is focused annularly onto a shroud coaxially located around the spike. Because the laser beam is focused by the nozzle surface, the nozzle geometry determines the power density of the laser pulse on the spot; then, it also determines the energy efficiency in generating a blast wave. Simultaneously, the nozzle contour defines the exhausting flow induced by the blast wave, and it determines the energy conversion from the blast-wave energy to the thrust work.

As for the energy efficiency in generating a blast wave, first of all, it is well known that plasma can be created on a nonablative surface at the power density of the order of 10^6 W/cm^2, whereas the power density of the order of 10^{10} W/cm^2 is required for air breakdown in the standard air atmosphere [10]. For the laser plasma generated on a nonablative surface, fluid dynamics [11–14], thermal coupling [11,13], ignition mechanisms [10,15,16], and momentum coupling [4,17] have been investigated. In some of these studies, the impulse generated on a flat disk surface was analyzed on the basis of the self-similar solution for the blast wave assuming the plasma as a point source. According to the self-similar solution, the impulse is determined by the energy in the point source. However, the energy conversion efficiency from the laser pulse energy to the point source energy has not been defined explicitly in previous studies. Authors introduced the blast-wave energy efficiency η_{bw} that is the fraction of E_i that is converted to the blast-wave energy E_{bw} [18]. Here, E_{bw} is the total amount of the internal and kinetic energies inside a blast wave. For the energy loss in generating a blast wave, a large amount of the energy is dissipated by radiation emission from the plasma. The other significant fraction of energy loss is the chemical potential and the electric excitation energy confined within the plasma that

Received 31 August 2009; revision received 12 July 2010; accepted for publication 14 July 2010.

*Lecturer, Department of Aerospace Engineering, Furo-cho, Chikusa-ku. Member AIAA.
†Research Associate, Department of Mechanical Engineering, 2-16-1 Tokiwadai, Ube. Member AIAA.

remains near the center of the expansion of the blast wave: it is inconvertible to thrust work, and it is gradually dissipated in the form of radiation. A function of the laser pulse shape and the spot size of the laser beam is $\eta_{\rm bw}$. It is natural to expect that there is the optimum range of the laser fluence that maximizes $\eta_{\rm bw}$ for a given laser pulse shape. Although the plasma development processes are inherently too complicated to characterize using a single parameter, the plasma can be treated as an infinitesimally small source of explosion in most cases when we are interested in the blast-wave expansion in a nozzle that is sufficiently larger than the typical size of the plasma [18]. The late-time energy conversion processes from the blast-wave energy to the thrust work can be treated as purely gas-dynamical problems. It can be solved with the help of the simple computations once $\eta_{\rm bw}$ is given.

Moreover, in order to achieve the stable flight of a vehicle, tolerance of the thrust performance to the optical misalignment is another important factor in designing the nozzle geometry. During the flight, the misalignment occurs due to the errors in the control of the positions and the orientations of the laser beam relative to the vehicle. The nozzle should be designed to keep the thrust automatically, even in such misaligned conditions. A "lightcraft" with a spike nozzle holds the altitude record by virtue of its "beam-riding" character, with which the vehicle retains the flight trajectory along the laser beam [1,19–21]. In the lightcraft with a parabolic nozzle, an ignition pin is used to keep the performance even in the misaligned conditions [22]. Experimental and theoretical investigations are still continuing today to achieve the stable flight. The flight dynamics are strongly dependent on the nozzle geometry, and experimental data are demanded to design the nozzle geometry suited for the actual flights.

What is the best nozzle shape that attains the maximum $\eta_{\rm bw}$ and C_m, even in the optically misaligned conditions? Innovations must be proposed. In the present study, we shall introduce a sharp cone as a good focusing optic, as well as an efficient gas-dynamical nozzle. The laser beam is concentrated through multiple reflections inside of a cone. Plasma is created on a surface interior of the cone; then, the impulsive thrust is generated. In the following section, the theory of the beam concentration in an axisymmetric cone is described. The stepwise distribution of the laser energy density on the surface of the cone is formulated in ideal conditions without the optical misalignment. The prospective advantages of the cone shape are described as well. In Sec. III, the experimental and computational methods are described. In Sec. IV, the experimental results of the impulse measurements are compared with the computational results to infer $\eta_{\rm bw}$. For the detailed discussions, the energy efficiency in generating a blast wave on an aluminum surface is measured in a simplified experimental setup. Moreover, the tolerance of the thrust performance to the deviation of the beam incident angle is investigated as well.

II. Principle of Beam Concentration in a Cone

Laser beam focusing inside of a cone is illustrated in Fig. 1. A cylindrical laser beam is incident on the base of the cone in the direction parallel to the center axis of the cone. The cross-sectional area of the laser beam is close to the base area of the cone. The inner surface of the cone has a mirror finish. Figure 1a illustrates a ray of the laser beam on its beam edge. The ray is reflected several times on the inner surface of the cone advancing toward the apex. The ray is reflected first at $P0$ and is directed toward the axis of symmetry. On the axis, the ray crosses another ray that is originated from a point that is rotationally symmetric to $P0$. This new ray, in turn, goes toward the surface and is then reflected at point $P1$. The angle between the chord of the cone and the ray is α_c at $P0$, and it becomes $3\alpha_c$ at $P1$, increasing by $2\alpha_c$. The angle at the jth reflection point, $P(j-1)$, is

$$\alpha_j = (2j-1)\alpha_c; \qquad (j = 1, 2, \ldots) \tag{1}$$

In Figs. 1a–1e, α_c is set at 10°, whereas in Fig. 1f, it is 4°, which is chosen for the experiment.

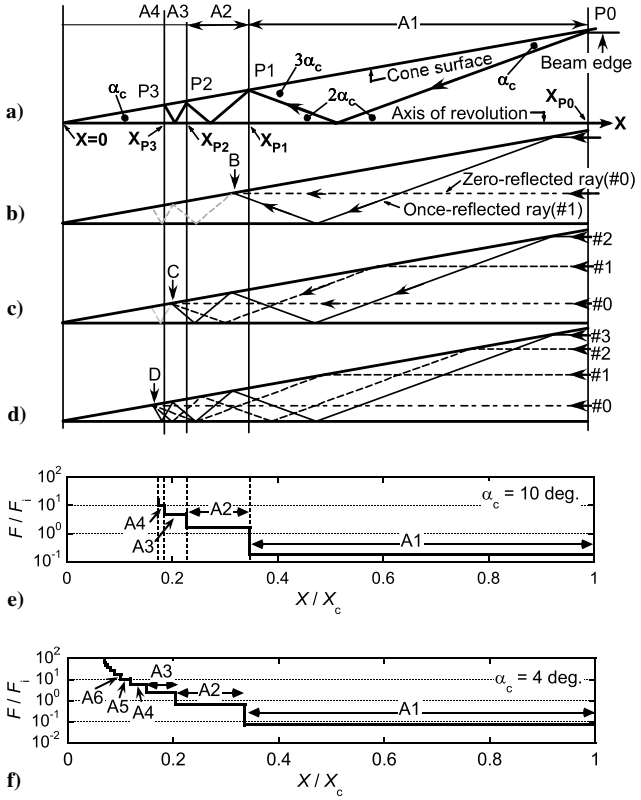

Fig. 1 Schematic for (a–d) the rays of the laser beam propagating in a cone, e) laser fluence on the cone surface for $\alpha_c = 10°$, and f) laser fluence for $\alpha_c = 4°$.

The laser fluence on the inner surface of the cone F changes in incremental steps. Figures 1b–1d are illustrated to explain the procedure to calculate the distribution of F. The reflection points of the ray on the beam edge, $P0$, $P1$, $P2$, $P3$, and so on, as illustrated in Fig. 1a, divide the cone surface into zones $A1$, $A2$, $A3$, and so on, that have different F. F on a surface in zone $A1$, F_{A1}, is uniform over zone $A1$, because only the zero-reflected rays reach zone $A1$, and it is simply formulated as

$$F_{A1} = F_i \sin\alpha_c \tag{2}$$

On a surface in zone $A2$, two rays, a once-reflected ray and a zero-reflected ray, are superimposed at a point, as illustrated in Fig. 1b. Hence, F changes at $P1$ in a stepwise manner (see Fig. 1a). For the axial position of point $P1$, X_{P1}, the radius of the open base of the cone is calculated in two ways as follows:

$$X_{P0}\tan\alpha_c = (X_{P0} - X_{P1})\tan 2\alpha_c - X_{P1}\tan\alpha_c \tag{3}$$

This leads to the following formula:

$$\frac{X_{P1}}{X_{P0}} = \frac{\tan 2\alpha_c - \tan\alpha_c}{\tan 2\alpha_c + \tan\alpha_c} \equiv r_1 \tag{4}$$

It is straightforward to extend this formula for the general point Pk:

$$\frac{X_{Pk}}{X_{P(k-1)}} = \frac{\tan(\alpha_{k+1} - \alpha_c) - \tan\alpha_c}{\tan(\alpha_{k+1} - \alpha_c) + \tan\alpha_c} \equiv r_k; \qquad (k = 1, 2, \ldots) \tag{5}$$

On a surface in zone $A2$, two rays are superimposed, and the fluence in this zone F_{A2} is formulated as

$$F_{A2} = F_i \sin(\alpha_c)\left(1 + \frac{1}{r_1^2}\right) \tag{6}$$

On a surface in zone $A3$, three rays (i.e., 0, 1 and 2) are superimposed, as illustrated in Fig. 1c. On a surface in zone $A4$, four rays are

Table 1 Laser fluence on the wall surface for $F_i = 1$ J/cm^2

Zone	F, J/cm^2	
	$\alpha_C = 4°$	$\alpha_C = 10°$
$A1$	0.07	0.17
$A2$	0.69	1.61
$A3$	2.37	4.99
$A4$	5.53	10.08
$A5$	10.48	15.84
$A6$	17.40	N/A

superimposed, as in Fig. 1d. In the same manner, the fluence on a surface in the Nth zone, AN, is formulated as

$$F_{\mathrm{AN}} = F_i \sin(\alpha_c)\left(1 + \frac{1}{r_1^2} + \frac{1}{r_1^2 r_2^2} + \cdots + \prod_{j=1}^{N-1} \frac{1}{r_j^2}\right)$$

$$= F_i \sin(\alpha_c)\left(1 + \sum_{k=1}^{N} \prod_{j=1}^{k-1} \frac{1}{r_j^2}\right) \tag{7}$$

The axial distribution of F is shown for $\alpha_c = 10°$, in Fig. 1e, and for $\alpha_c = 4°$, in Fig. 1f.

The number of the reflection has the maximum limit. In each reflection, α_j increases by $2\alpha_c$; then, it finally exceeds 90° after a certain number of the reflection. The rays start to return toward the open base of the cone. The maximum number of the reflection $N_{\max}$ is the natural number satisfying

$$N_{\max} \le \frac{1}{2}\left\{\frac{90°}{\alpha_c} - 1\right\} \tag{8}$$

The maximum fluence $F_{\max}$ is calculated as $F_{\max} = F_{AN_{\max}}$. As shown in Fig. 1e, for α_c at 10°, $F_{\max}/F_i$ is around 15. It is sensitive to α_c. $F_{\max}/F_i$ is 77 for $\alpha_c = 4°$, as shown in Fig. 1f. In Table 1, the laser fluence in each zone is presented in the case of $F_i = 1$ J/cm^2, which is typical in experiments. The laser pulse duration is around 1 μs. Because plasma is created at a laser power density larger than 10^6 W/cm^2, it is natural to expect that plasma is ignited when F exceeds 1 J/cm^2. Plasma is ignited on a surface in zone $A3$ for $\alpha_C = 4°$. It occurs in zone $A2$ for $\alpha_C = 10°$.

Conical nozzles have several favorable features:

1) After the plasma is first created on a surface (say, in zone $A2$), some fraction of the laser energy is reflected without being absorbed by the plasma. The reflected laser beam reaches the surface in the deeper zone $A3$ to create plasma, contributing to the thrust generation.

2) Plasma is created at moderate fluence close to the plasma ignition threshold, as shown in Table 1. Otherwise, the plasma is created at large fluence, and a large amount of the laser energy is lost due to radiation emission from the plasma as it looses η_{bw}.

3) Plasma is generated in the deep zones of the nozzle. According to a previous study by Katsurayama et al. [9], when the plasma is generated near the nozzle exit, C_m becomes lower, as compared with the case when the plasma is generated near the apex, because the nozzle is not used effectively to confine the blast wave.

4) Generation of the plasma on the surface should be useful for the nozzle cooling.

5) By virtue of geometrical simplicity, the lightweight cone can be easily manufactured.

These prospects should be verified in the experiments, because it is difficult to predict the thrust performance from only the simple geometrical considerations. The plasma is generated on the surfaces over the multiple zones ($A4$, $A5$, $A6$, etc.). The laser absorption by the plasma in the frontal zones changes the distribution of F in the deeper zones from what is shown in Fig. 1f. In addition to the impulse measurement, the relation between η_{bw} and F must be clarified.

In previous studies by Mori et al. [8] and Katsurayama et al. [9], it was found that the impulse increases with decreasing α_C. Hence, it is natural to expect that a high impulse is obtained with a low-α_C nozzle: that is, a sharp-cone nozzle. In addition, F is significantly larger for $\alpha_C = 4°$ than for $\alpha_C = 10°$. These reasons are why we chose $\alpha_C = 4°$ for the experiments.

III. Methods

A transversely excited atmospheric CO_2 pulse laser [8,18,23] is used in the experiments. The laser pulse shape is a leading-edge spike followed by an exponentially decaying tail. The full width at the half maximum of the spike is 120 ns. The tail lasts for around 3 μs, and its decay constant is 1.3 μs. The laser pulse energy E_i is varied from 4 to 11 J. The energy distribution is approximately flat over the cross section. The cross section of the laser beam is a square of 26 mm. The laser fluence of the original, not the focused, beam F_i is 0.6 J/cm^2 at a minimum for $E_i = 4$ J. It is 1.6 J/cm^2 at the maximum for $E_i = 11$ J. The conical nozzle is made of an aluminum sheet of 0.5 mm thickness. The surface of the aluminum sheet has a mirror finish. Its half-divergence angle α_c and the chord length L_n are 4° and 200 mm, respectively. The diameter of its open base is 28 mm, whereas the cross section of the laser beam is a square of 26 mm. Most of the laser energy enters through the open base of the cone. The direction of the laser beam is exactly aligned with the axis of the cone.

The impulse generated in the conical nozzle is measured using a ballistic pendulum [8], as shown in Fig. 2. The pendulum oscillation is monitored using a laser displacement sensor (Keyence, Inc., LK-500). For the calibration of the pendulum sensitivity, an impulse hammer is used to generate an impulse to the pendulum. The impulsive force from the hammer to the pendulum is measured using a force sensor (PCB Piezotronics, Inc.) attached on the hammerhead. Simultaneously, sinusoidal oscillation of the pendulum is monitored using the displacement sensor. The impulse is proportional to the maximum displacement of the pendulum. The scattering of the measured impulse from the correlation line is less than 1%. The measurement of the laser impulse is conducted more than five times for each condition.

To interpret the experimental results in the sense of energy efficiency, computations are conducted. A cell-centered finite-volume scheme is adopted to solve axisymmetric Navier–Stokes equations. Air is treated as an ideal gas. Inviscid flux is estimated using the AUSM-DV scheme [24], and its space accuracy is extended to third order using the MUSCL approach with Edwards's pressure limiter [25]. Viscous and heat fluxes are estimated using a standard central difference, in which the viscosity and thermal conductivity of air are estimated using Sutherland's formula. Time integration is performed using the LU-SGS scheme [26] extended to third-order time accuracy by Matsuno's inner iteration method [27]. The computation is performed using Courant–Friedrichs–Lewy numbers of 2–50. Figure 3 shows the computational grid and a close-up image of it. The grid inside of the nozzle is so fine that no grid dependence was observed for the shock propagation speed and resulting thrust. Its axial resolution is uniformly $\Delta R_n = 126$ μm. The outer boundary is set far from the nozzle for the computed results, so as to not be affected by the nonphysical waves reflected from the boundary. The

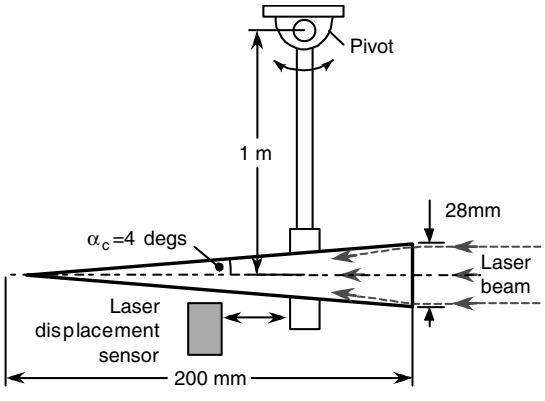

Fig. 2 Schematic for impulse measurement setup.

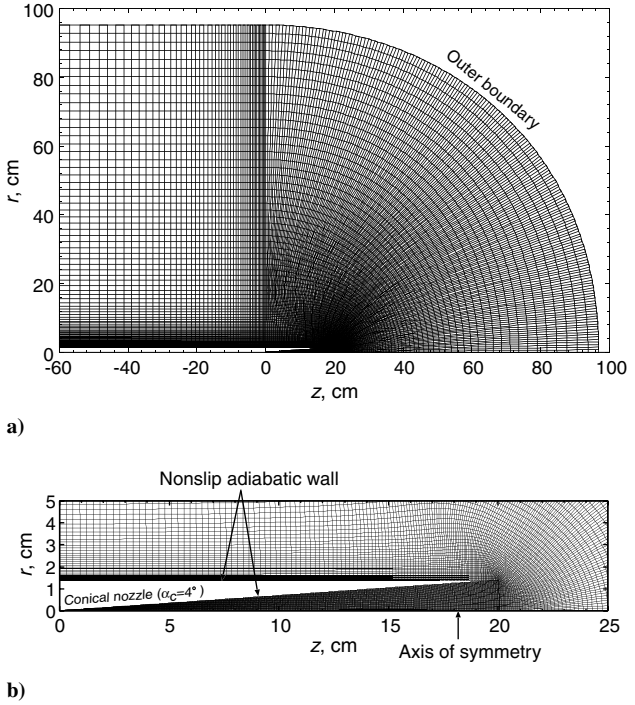

Fig. 3 Computation grid: a) overall view and b) close-up view.

nonslip and adiabatic conditions are imposed on the nozzle wall, because heat flux from the rarefied plasma to the wall has already been excluded through exclusion of the remaining energy, which is inconvertible to drive a blast wave. In addition, the heat flux from the shock layer to the wall is negligible, because the Mach number of the adiabatically expanding blast wave is less than Mach 2. On the outer boundary, if the flow is a supersonic outflow, the primitive values are zeroth extrapolated from inner grids. If the flow is subsonic regardless of outflow and inflow, the pressure on the boundary is specified to the ambient pressure, and other primitive values are zero extrapolated.

For the initial conditions, a spherical source of the blast wave is placed at the apex of the nozzle surrounded by the standard air atmosphere. The radius of the source point is 1 mm. The air density in the source is equal to that in the ambient atmosphere. The pressure inside of the source is determined as $(\gamma-1)E_{\rm bw}/V_{\rm source}$, where $V_{\rm source}$ represents the volume of the source, and the internal energy inside of the source is equal to $E_{\rm bw}$, which is parametrically changed to reproduce the dependency of C_m on $E_{\rm bw}$. The present computation code was originally built to verify the experimental results in a previous study by Katsurayama et al. [9]. The present study aims to estimate $\eta_{\rm bw}$ from the experimentally measured C_m while the detailed short-term phenomena are ignored. The influence of finite spacial extent of the plasma is ignored as well. In the experiment, the plasma is created, not in an infinitesimally small volume of sphere, but on a surface of a finite area. The expansion of the blast wave at the initial stage is more complicated than that assumed in the computation. According to the previous study by Katsurayama et al. [9], the effect of the finite extent of the plasma was found dependent on α_c. For the conical nozzles of α_c larger than 30°, the discrepancy between the experiment and the computation was more than 10%, while it was less than 5% for α_c smaller than 10°. It is natural to expect that the plasma size effect is ignorable for the nozzles of α_c smaller than 10° and of a sufficiently large size.

IV. Results and Discussions

A. Impulse

Figure 4 shows the relation between C_m and E_i. Closed circles represent the experimental results, and open circles represent the computational results. The experimental C_m increases monotonously with E_i. The maximum C_m is around 0.3 mNs/J. This value is

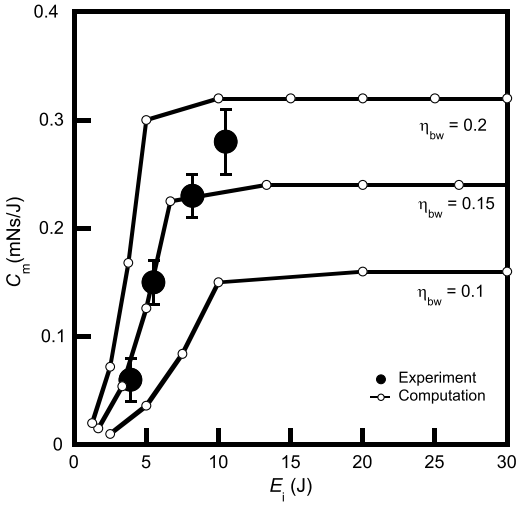

Fig. 4 Relation between C_m and E_i for the sharp-cone nozzle with $\alpha_C = 4°$ in the optically aligned condition.

relatively high compared with the experimental results for different nozzle geometries [1–9]. Computation results are also plotted in the figure. According to previous experimental studies for conical nozzles [7,9], C_m has the maximum peak for the dimensionless nozzle length,

$$\tilde{r}_n[\equiv L_n/\sqrt[3]{2\eta_{\rm bw}E_i/p_a(1-\cos\alpha_c)}] = 0.41$$

Assuming that $\eta_{\rm bw} = 0.2$, $L_n = 200$ mm, $\alpha_c = 4°$, and $E_i = 11$ J, $\tilde{r}_n$ is calculated at 0.77, still larger than the optimum value, 0.41. It is clear from the definition of $\tilde{r}_n$ that $\tilde{r}_n$ decreases with E_i if $\eta_{\rm bw}$, L_n, and α_c are kept constant. When E_i increases to 72 J, $\tilde{r}_n$ will reach the optimum value. From this perspective, the present trend, in which C_m increases with E_i, seems natural. Further discussions should be accompanied with detailed data of the energy efficiency. We shall at first compare the experimental C_m-E_i curve with the computational results to infer $\eta_{\rm bw}$ in the present experiments.

Figure 5 shows computed pressure contours for $E_{\rm bw} = 0.75$ J. Hereafter, Δp in the caption represents the pressure interval between the adjacent two contours. After the point source is ruptured at $t = 0$, a strong shock wave propagates toward the nozzle exit. After $t = t_0$,

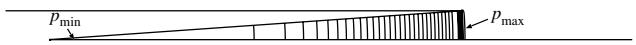

a) t = 315 μs =t_0. (p_{max} = 1.42 atm, p_{min} = 8.24×10^{-1} atm, Δp=1.98×10^{-2} atm)

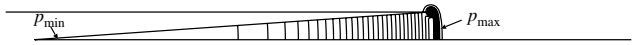

b) t = 325 μs =t_1. (p_{max} = 1.40 atm, p_{min} = 8.30×10^{-1} atm, Δp=1:91×10^{-2} atm)

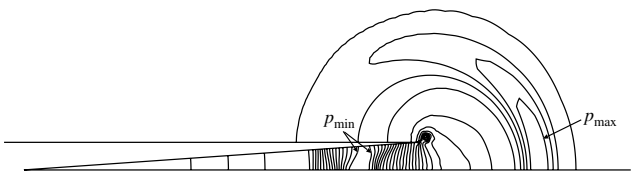

c) t = 485 μs =t_2. (p_{max} = 1.04 atm, p_{min} = 7.32×10^{-1} atm, Δp=1.04×10^{-2} atm)

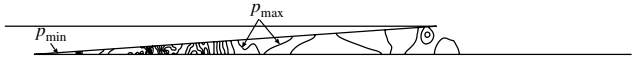

d) t = 880 μs =t_3. (p_{max} = 1.12 atm, p_{min} = 4.29×10^{-1} atm, Δp=2.31×10^{-2} atm)

Fig. 5 Computational results (pressure contour for $E_{\rm bw} = 0.75$ J) (atm denotes standard atmosphere).

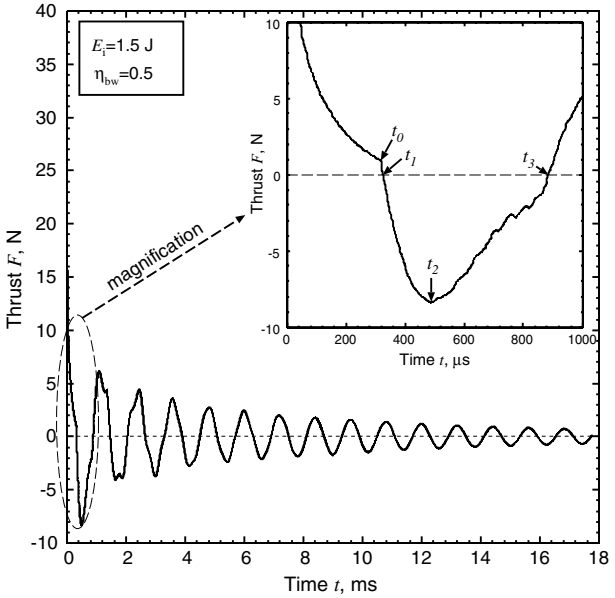

Fig. 6 Computational result (thrust history).

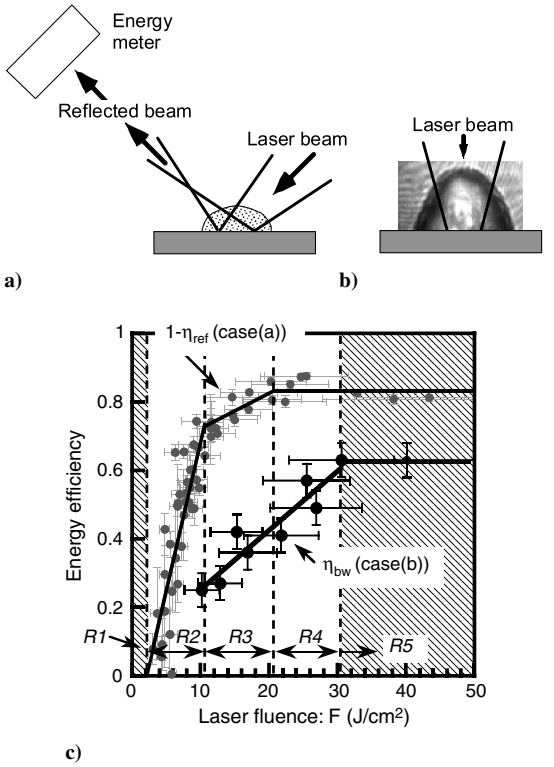

Fig. 7 Energy balance for the surface plasma: a) setup for the measurement of 1-η_{ref} (45° incidence), b) setup for the measurement of η_{bw} (normal incidence), and c) influence of the laser fluence F on 1-η_{ref} and η_{bw}.

at which the shock wave reaches the nozzle exit (see Fig. 5a), the compressed air starts to be exhausted. Figure 6 shows the temporal change in the thrust to the nozzle. Large impulsive positive thrust is generated until $t = t_0$. Thrust decreases to zero at $t = t_1$, soon after the shock wave blasts off the nozzle exit, as shown in Fig. 5b. Then, the rarefaction waves behind the shock wave sweep out the inside of the nozzle. Thrust takes the minimum value at $t = t_2$, at which time the gauge pressure becomes negative for the entire region inside of the nozzle, as shown in Fig. 5c. After $t = t_2$, the pressure inside of the nozzle begins to recover. Thrust reverts to zero at $t = t_3$ when the mean pressure inside is in equilibrium with the atmospheric pressure. However, as shown in Fig. 5d, the detailed pressure distribution is too complex to interpret. Rarefaction waves associated with a vortex are generated around the nozzle tip, and these waves again propagate into the inside of the nozzle, which invokes a complex refilling process. As shown in Fig. 6, the thrust oscillates around zero, and the oscillation attenuates gradually after $t = t_3$. Although the majority of the impulse should be originated from the thrust generated until 1 ms, the oscillating thrust that continues for more than 10 ms is not negligible for the precise estimation of the impulse. Computations are continued until $t = 10$ ms, and the thrust history is integrated with the time to calculate the impulse.

In the computation, E_{bw} is varied as a parameter. The impulse is calculated as a function of E_{bw}, and then a E_{bw}-impulse curve is uniquely drawn. Then, similar computational curves are drawn for different values of η_{bw} on the E_i-C_m plane in Fig. 4. The computed C_m increases monotonously with E_i, and then a plateau appears at a certain E_i that corresponds to $E_{bw} = 1$ J. For example, the computational curve of $\eta_{bw} = 0.1$ reaches the inflexion point at $E_i = 10$ J that corresponds to $E_{bw} \equiv \eta_{bw} E_i = 1$ J. The computational curve of $\eta_{bw} = 0.15$ agrees well with the experimental plots for $E_i < 8$ J. Experimental C_m for $E_i > 8$ J is in between two curves of $\eta_{bw} = 0.15$ and $\eta_{bw} = 0.2$. This η_{bw} is much lower than that for the air breakdown, which is around 0.4 [18].

B. Energy Efficiency

From the geometrical consideration, the stepwise distribution of F on the surface of the cone is deduced. In the foregoing experiments, η_{bw} is presumed as low as 0.15. We then investigate the relation between η_{bw} and F in the other experimental setup. The laser beam is focused using a Zn–Se lens, for which the focal length is 200 mm, onto an aluminum surface with a mirror finish. F, on the surface, is controlled by varying E_i and the spot diameter. The fraction of the incident laser pulse energy that is reflected on the surface η_{ref} is measured using an energy meter, as illustrated in Fig. 7a. The laser beam is obliquely incident onto the surface, with the incident angle at 45°. The laser beam is partly absorbed by the surface plasma, and the remainder is specularly reflected. The cross-sectional diameter and the position of the reflected beam are monitored using thermal papers. By taking schlieren pictures of the blast wave expanding around the surface plasma, η_{bw} is measured [18]. For this measurement, the laser beam is normally incident onto the surface, as illustrated in Fig. 7b. The measurement is performed five times for each condition.

Figure 7c shows the absorption efficiency defined as 1-η_{ref} measured in the setup (Fig. 7a) and η_{bw} measured in the setup (Fig. 7b). The scattering of F is evaluated from the variation of E_i and the uncertainty of the spot size on the target surface. The scatterings of 1-η_{ref} and η_{bw} are evaluated from the standard deviation of the data that should be originated from both the scattering of E_i and from the scattering in the surface roughness due to the beam irradiation. The present 1-η_{ref} curve is similar to that for a relatively short 175 ns pulse [17]. The energy efficiencies are sensitive to F, and they can be categorized into five regimes, $R1$–$R5$, as shown in the figure. In regime $R1$, at $F < 2$ J/cm^2, 1-η_{ref} is close to zero. For the wavelength at 10.6 μm, the intrinsic η_{ref} of aluminum is 0.99 for the surface temperature at 300 K [17]. Evaporation should never occur in this regime. The surface temperature is kept lower than the vaporization temperature. The absorbed fraction of the laser energy dissipates in the volume of the aluminum target. There seems to be scattering with the critical value of F around 2 J/cm^2. In regime $R2$, at $2 < F < 10$ J/cm^2, 1-η_{ref} increases sharply with F. Plasma was observed on the surface, whereas η_{bw} could not be extracted because the blast wave was very weak. In this regime, η_{bw} is presumed less than 0.2. Once the plasma is created, the laser power is absorbed in the plasma. The plasma is onset from the vaporization of the surface [16]. In regime $R2$, only the initial part of the laser pulse is reflected during the period necessary to heat the metal surface to the vaporization temperature. Hence, it should be noted that the critical laser fluence and the slope of the 1-η_{ref} curve in regime $R2$ are dependent on the laser pulse shape as well as F. In regime $R3$, at $10 < F < 20$ J/cm^2, the slope of increasing 1-η_{ref} becomes moderate. In

regimes $R4$ and $R5$, at $F > 20$ J/cm^2, 1-η_{ref} saturates to be around 0.8, whereas η_{bw} is still increasing in regime $R4$ until it becomes constant in regime $R5$. In regime $R5$, η_{bw} is around 0.6, and this value is higher than η_{bw} for air breakdown (around 0.4) [18]. The thermal coupling of the laser energy to the solid target has its peak around the power density corresponding to the plasma ignition threshold [16]. This suggests that the energy dissipation to the solid volume becomes the maximum in regime $R2$, where the laser fluence is close to the plasma ignition threshold. In regimes $R3$ and $R4$, the thermal coupling should still be significant, although the amount of the energy lost in the solid volume should decrease with increasing F. The trend through regimes $R2$ to $R4$ is originated from the transition of the laser absorption mechanisms. It is well known that the laser absorption occurs through different mechanisms, depending on the laser power density. At a laser power density lower than 10^6 W/cm^2, the laser-supported combustion (LSC) wave [4,10–12,17,23,28] is generated. At a laser power density higher than 10^7 W/cm^2, the laser-supported detonation (LSD) wave should occur to absorb the laser energy efficiently in a dense plasma behind a precursor shock wave. The laser pulse duration is the order of 1 μs in the present experiment. The LSD wave mechanism should be prevailing against the LSC wave mechanism in regimes $R3$ and $R4$. In regime $R5$, the LSD wave is dominant throughout the plasma developing processes.

On the basis of Table 1 and Fig. 7c, we shall verify the estimation of η_{bw} ($\sim$0.15) for the inside of the cone. From Table 1, F exceeds the threshold around 2 J/cm^2 slightly on the surface in zone $A3$. Most of the laser energy is reflected throughout the zones between $A1$ and $A3$, and then it is transmitted to zone $A4$ where plasma is first created with $F = 5.53$ J/cm^2 (see Fig. 7c). For $F = 5.53$ J/cm^2, 1-η_{ref} is still as low as 0.4, and η_{bw} should be less than 0.2. Approximately 40% of the incident laser energy is absorbed in the plasma, and the remainder, 60%, reaches zone $A5$. Because of the absorption in $A4$, F becomes $0.6 \times 10.48 \sim 6.3$ J/cm^2 on a surface in zone $A5$ (see Fig. 7c again). For $F = 6.3$ J/cm^2, 1-η_{ref} is around 0.4, and η_{bw} is less than 0.2, again. Then, 36% of the initial laser energy reaches zone $A6$. This leads to $F \sim 0.36 \times 17.4 \sim 6.3$ J/cm^2 in $A6$. After all, in the present experimental condition, η_{bw} is kept less than 0.2 over the entire region where plasma is ignited. Higher η_{bw} is attainable at higher F_i. For example, for $F_i = 30$ J/cm^2, F is 2.1 J/cm^2 in $A1$, 20.7 J/cm^2 in $A2$, 66 J/cm^2 in $A3$, and 165 J/cm^2 in $A4$, according to Table 1. Plasma is generated on a surface in zone $A2$ with 1-$\eta_{\text{ref}} \sim 0.8$ and $\eta_{\text{bw}} \sim 0.5$.

C. Performance in a Misaligned Condition

The tolerance of the conical nozzle to the optical misalignment is investigated in the other setup. The laser beam is irradiated obliquely to the nozzle exit plane. Figure 8 shows the experimental C_m as a function of the incident angle of the laser beam to the nozzle exit plane θ_i for $E_i = 11$ J. C_m is as much as 0.3 Ns/mJ at $\theta_i = 0°$. C_m decreases gradually to 0.2 Ns/mJ at $\theta_i = 10°$. The C_m-θ_i incidentally coalesces to a Gaussian curve for which the half width at half maximum (HWHM) is 11°. This value is dependent on F_i and α_c.

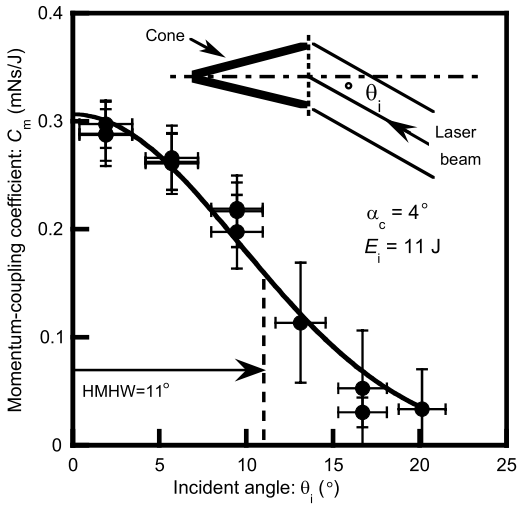

Fig. 8 Misalignment effect: relation between C_m and θ_i for the sharp-cone nozzle with $\alpha_c = 4°$.

The beam cross-sectional area that is projected on the nozzle exit plane increases with θ_i. It may be concerning that some fraction of the laser energy may not enter the cone for large θ_i. However, the beam cross section is kept centered at the axis of the cone, and the increments in the beam cross-sectional area are only 6%, even for $\theta_i = 20°$. Hence, it is negligible in the present experiment. In the misaligned conditions, the ray trace becomes asymmetric and complicated. The distribution of F becomes nonuniform in the azimuthal direction. F should be reduced over the whole area. This leads to inefficient generation of the plasma. Further analysis requires three-dimensional ray tracing and plasma modeling that are far above the present scope.

The present C_m-θ_i curve is similar to the experimental results for a parabolic nozzle. In a flight experiment of a lightcraft with a parabolic nozzle [22], C_m is analyzed with respect to the initial lateral offset and the tilt angle of the vehicle relative to the laser beam. In a manner similar to the present results, C_m changes with θ_i along a Gaussian curve. It is reported that the significant decrease in C_m occurs at $\theta_i = 8.5°$. This value is close to, but slightly smaller than, the present result of the HWHM at $\theta_i = 11°$. For a lightcraft with a spike nozzle [20,21], the misalignment effects are reported only with regard to the initial lateral offset. Unfortunately, the authors could not find any data sets that could be compared with the present result.

V. Conclusions

A sharp cone is employed as a nozzle for pulsed laser propulsion. The laser beam is concentrated through the multiple reflections on the inner surface of the cone, and laser fluence on the inner surface increases along the axis of symmetry in an incremental manner. Plasma is created on a surface deep inside of the cone, where the laser fluence exceeds the threshold. In the experiment, it is found that a large momentum-coupling coefficient, 0.3 mNs/J, is attainable. For the energy efficiency, the blast-wave energy efficiency is estimated to be around 0.15 by comparing the measured impulse with the computed impulse. The estimated value of the efficiency is supported qualitatively on the basis of the ray-tracing analysis and the measurement of the energy efficiency in a simplified setup. Moreover, the present nozzle geometry is found to be tolerant to the optical misalignment; the HWHM of the C_m-θ_i curve is 11° in the present experimental condition.

Acknowledgments

The authors are grateful to Kimiya Komurasaki and Yoshihiro Arakawa at the University of Tokyo for mutual discussions on the results.

References

[1] Myrabo, L. N., "World Record Flights of Beamed-Riding Rocket Lightcraft," AIAA Paper 2001-3798, 2001.

[2] Rezunkov, Yu. A., Safronov, A. L., Ageichik, A. A., Egorov, M. S., Stepanov, V. V., Rahuk, V. S., Guterman, V. Yu., Ivanov, A. V., Rebrov, S. G., and Golikov, A. N., "Performance Characteristics of Laser Propulsion Engine Operating both in CW and in Repetitively-Pulsed Modes," *Proceedings of the Fourth International Symposium on Beamed Energy Propulsion*, AIP Conference Proceedings, Vol. 830, American Inst. of Physics, New York, 2006, pp. 3–13.

[3] Sasoh, A., "Laser in Tube Accelerator," *Review of Scientific Instruments*, Vol. 72, No. 3, 2001, pp. 1893–1898. doi:10.1063/1.1347378

[4] Pirri, A. N., Monsler, M. J., and Mebolsine, P. E., "Propulsion by Absorption of Laser Radiation," *AIAA Journal*, Vol. 12, No. 9, 1974, pp. 1254–1261. doi:10.2514/3.49462

[5] Myrabo, L. N., Libeau, M. A., Meloney, E. D., Bracken, R. L., and Knowles, T. B., "Pulsed Laser Propulsion Performance of 11-cm

Parabolic 'Bell' Engines Within the Atmosphere," AIAA Paper 2002-3783, May 2002.

[6] Mori, K., Sasoh, A., and Myrabo, L. N., "Pulsed Laser Propulsion Performance of 11-cm Prabolic 'Bell' Engines: CO2 TEA vs. EDL," *Proceedings of the Fourth International Symposium on Beamed Energy Propulsion*, Vol. 830, AIP Conference Proceedings, American Inst. of Physics, New York, 2006, pp. 38–47.

[7] Ageev, V. P., Barchukov, A. I., Bunkin, F. V., Konov, V. I., Korobeinikov, V. P., Putjatin, B. V., and Hudjakov, V. M., "Experimental and Theoretical Modeling of Laser Propulsion," *Acta Astronautica*, Vol. 7, No. 1, 1980, pp. 79–90. doi:10.1016/0094-5765(80)90119-8

[8] Mori, K., Komurasaki, K., Arakawa, Y., "Nozzle Scale Optimum for the Impulse Generation in a Laser Pulsejet," *Journal of Spacecraft and Rockets*, Vol. 41, No. 5, Sept.–Oct. 2004, pp. 887–889. doi:10.2514/1.5677

[9] Katsurayama, H., Komurasaki, K., Hirooka, Y., Mori, K., and Arakawa, Y., "Numerical Analyses of Exhaust and Refill Processes of a Laser Pulse Jet," *Journal of Propulsion and Power*, Vol. 24, No. 5, Sept.–Oct. 2008, pp. 999–1006. doi:10.2514/1.29087

[10] Weyl, G., Rollins, C., and Resendes, D., "Ignition and Maintenance of Laser-Supported Detonation Waves," *AIAA Journal*, Vol. 29, No. 5, May 1991, pp. 763–772. doi:10.2514/3.10652

[11] Pirri, A. N., Root, R. G., and Wu, P. K. S., "Plasma Energy Transfer to Metal Surfaces Irradiated by Pulsed Lasers," *AIAA Journal*, Vol. 16, No. 12, 1978, pp. 1296–1304. doi:10.2514/3.61046

[12] Maher, W. E., and Hall, R. B., "An Interferometeric Investigation of Laser-Supported Absorption Waves," *Journal of Applied Physics*, Vol. 46, No. 2, 1975, pp. 761–772. doi:10.1063/1.321642

[13] Ageev, V. P., Barchukov, A. I., Bunkin, F. V., Konov, V. I., Puzhaev, S. B., Silenok, A. S., and Chapliev, N. I., "Heating of Metals by CO_2 Laser Radiation Pulses," *Soviet Journal of Quantum Electronics*, Vol. 9, No. 1, 1979, pp. 43–47. doi:10.1070/QE1979v009n01ABEH008568

[14] Maher, W. E., and Hall, R. B., "Experimental Thermal Coupling of Laser Beams," *Journal of Applied Physics*, Vol. 49, No. 4, 1978, pp. 2254–2261. doi:10.1063/1.325132

[15] McMordie, J. A., and Roberts, P. D., "The Interaction of Pulsed CO_2 Laser Radiation with Aluminum," *Journal of Physics D: Applied Physics*, Vol. 8, No. 7, 1975, pp. 768–781. doi:10.1088/0022-3727/8/7/009

[16] Weyl, G., Pirri, A. N., and Root, R., "Laser Ignition of Plasma Off Aluminum Surfaces," *AIAA Journal*, Vol. 19, No. 4, 1981, pp. 460–469. doi:10.2514/3.50968

[17] Reilly, J. P., Ballantyne, A., and Woodroffe, J. A., "Modeling of Momentum Transfer to a Surface by Laser-Supported Absorption Waves," *AIAA Journal*, Vol. 17, No. 10, 1979, pp. 1098–1105. doi:10.2514/3.61283

[18] Mori, K., Komurasaki, K., and Arakawa, Y., "Energy Transfer from a Laser Pulse to a Blast Wave in Reduced-Pressure Air Atmosphere," *Journal of Applied Physics*, Vol. 95, No. 11, 2004, pp. 5979–5983. doi:10.1063/1.1710721

[19] Libeau, M., and Myrabo, L., "Off-Axis and Angular Impulse Measurements on a Lightcraft Engine," *Proceedings of the Third International Symposium on Beamed Energy Propulsion*, Vol. 766, AIP Conference Proceedings, American Inst. of Physics, New York, 2005, pp. 166–177.

[20] Libaeu, M. A., Myrabo, L. N., Filippelli, M., and McInerney, J., "Combined Theoretical and Experimental Flight Dynamics Investigation of a Laser-Propelled Vehicle," *AIP Conference Proceedings*, Vol. 664, American Inst. of Physics, New York, 2003, pp. 125–137.

[21] Ballard, C. G., Anderson, K. S., and Myrabo, L., "Flight Dynamics and Simulation of Laser Propelled Lightcraft," *Journal of Computational and Nonlinear Dynamics*, Vol. 4, No. 4, 2009, Paper 041005. doi:10.1115/1.3187214

[22] Scharring, S., Hoffmann, D., Eckel, H.-A., and Roser, H.-P., "Stabilization and Steering of a Parabolic Laser Thermal Thruster with an Ignition Device," *Acta Astronautica*, Vol. 65, Nos. 11–12, 2009, pp. 1599–1615. doi:10.1016/j.actaastro.2009.04.007

[23] Mori, K., Komurasaki, K., and Arakawa, Y., "Influence of the Focusing f Number on Heating Regime Transition in Laser Absorption Waves," *Journal of Applied Physics*, Vol. 92, No. 10, 2002, pp. 5663–5667. doi:10.1063/1.1513869

[24] Wada, Y., and Liou, M. S., "A Flux Splitting Scheme with High-Resolution and Robustness for Discontinuities," NASA TM 106452, 1994.

[25] Edwards, J. R., "A Low-Diffusion Flux-Splitting Scheme for Navier-Stokes Calculations," *Computers and Fluids*, Vol. 26, No. 6, 1997, pp. 635–659. doi:10.1016/S0045-7930(97)00014-5

[26] Jameson, A., and Yoon, S., "Lower-Upper Implicit Schemes with Multiple Grids for the Euler Equations," *AIAA Journal*, Vol. 25, No. 7, 1987, pp. 929–935. doi:10.2514/3.9724

[27] Matsuno, K., "Actual Numerical Accuracy of an Iterative Scheme for Solving Evolution Equations with Application to Boundary-Layer Flow," *Transactions of the Japan Society for Aeronautical and Space Sciences*, Vol. 38, No. 122, 1996, 2002, pp. 311–322.

[28] Raizer, Y. P., *Laser-Induced Discharge Phenomena*, Consultants Bureau, New York, 1977, Chap. 6.

G. Spanjers
Associate Editor